ORIGINAL RESEARCH　　　　　　　　　　　　　　　　　　　**Open Access**

A generalized synthesis load model considering network parameters and all-vanadium redox flow battery

L Zhou[1], Z W Peng[1], C R Deng[1], X Z Qi[2]* and P Q Li[2]

Abstract

The simulation precision of the classic load model (CLM) is affected by the increasing proportion of installed energy storage capacity in the grid. This paper studies the all-vanadium redox flow battery (VRB) and proposes an equivalent model based on the measurement-based load modeling method, which can simulate the maximum output of the VRB energy storage system and fit the external characteristic of the system precisely in the occurrence of large disturbance and continuous small disturbance. The equivalent model is connected to CLM to form a generalized synthesis load model (GSLM), which considers the parameters of distribution network and reactive power compensation. Compared with CLM, GSLM has better structures and can describe the load characteristics of distribution network with energy storage system more precisely. Simulation results validate the effectiveness and good parameter stability of GSLM, and show that the higher the proportion of energy storage in the grid is the better description ability GSLM has.

Keywords: All-vanadium redox flow battery, Classic load model, Network parameter, Parameter identification, Reactive compensation

1 Introduction

Renewable clean energy is an important part of smart grid and energy Internet, but it must be combined with energy storage system to meet the requirements of a safe, stabile and efficient large power system. From the perspective of load modeling, the type, composition, and charging and discharging depth of the load model will directly affect the results of the study. Under critical conditions, different load models will lead to complete different simulation and calculation results [1–6]. Under this background, the load model used in the calculation of power system must include energy storage system. The commonly used load model in power system calculation includes induction motor and static load, and the static load is the combination of constant impedance, constant current and constant power loads. It is directly connected to the high voltage load bus and is called the classic load model (CLM) [7, 8]. In actual distribution systems, the load is usually connected to the medium and low voltage distribution buses, so CLM may amplify the effect of the motors, leading to errors in the load model. Therefore, developing better-structured load model is of great theoretical value and practical significance.

All-vanadium redox flow battery has attracted wide attention in industry for its noticeable advantages and has been used as energy storage system and operated with clean energy [9–12]. The model of VRB has been studied in many publications. A two-dimensional electrochemical model of VRB is established in [13], which considers the factors of chemical reaction kinetics and can accurately calculate the ion concentration and the dynamic distribution of potential with time and space. The model of VRB including fluid mechanics, electricity and electrochemical multiple physical fields is established in [14]. It uses Bernoulli equation, Nernst equation and some empirical equations to describe the relation between the battery parameters, and the numerical calculation model of the battery system is established from energy perspective. In [15, 16], a fourth-order dynamic model of the energy storage battery is established and further improved. The model

* Correspondence: 376563378@qq.com
[2]College of Electrical and Information Engineering, Hunan University, Changsha 410082, China
Full list of author information is available at the end of the article

Zhou *et al. Protection and Control of Modern Power Systems* (2018) 3:32

Page 2 of 13

takes into account the nonlinear characteristics of the charging and discharging processes, which have a complex structure with many parameters. The AC impedance model of VRB is established and improved in [17–20], which contains the reaction resistance, ohm impedance, pump damage and additional loss.

Based on the above research, a distribution network simulation model with VRB energy storage system is established in this paper, and the characteristics of the system are obtained at the grid connection bus. From the external characteristics, a simplified equivalent model of VRB energy storage system based on the measurement-based load modeling method is established, which can simulate the maximum output of the VRB energy storage system and fit the external characteristics of the system precisely in the presence of large disturbance and continuous small disturbance. In addition, the model has a simple structure and can be identified easily. The equivalent model is then connected to CLM to form a generalized synthesis load model (GSLM) which considers the parameters of distribution network and reactive power compensation. Compared with CLM, GSLM has better structure and can describe the load characteristics of distribution network with energy storage system more precisely.

This paper is organized as follows. The model of VRB energy storage system is established in Section 2. In Section 3, an equivalent model of the system is proposed from the principle of external characteristic equivalent fitting. In Section 4, GSLM is established, its parameters are identified, and simulation studies are carried out. Finally, Section 5 draws the conclusion.

2 VRB model and simulation of grid connected system

2.1 VRB model
VRB models are divided into electrochemical model and equivalent circuit model according to the principle of modeling. The mathematical equations of the former are complex requiring large amount of calculation, and the necessary micro parameters are difficult to obtain in modeling process. The latter model can directly reflect the external equivalent characteristics of the battery and the changes of various characteristic parameters in the process of charging and discharging are clear. An improved equivalent circuit model based on the assumption of loss [9–11, 18–20] is used in this paper, and the model structure is shown in Fig. 1.

As shown in Fig. 1, the controlled voltage source U_s is the open circuit voltage of the battery and U_b is the battery terminal voltage. R_{eac} and R_{es} represent the internal loss of the battery, which include the diaphragm
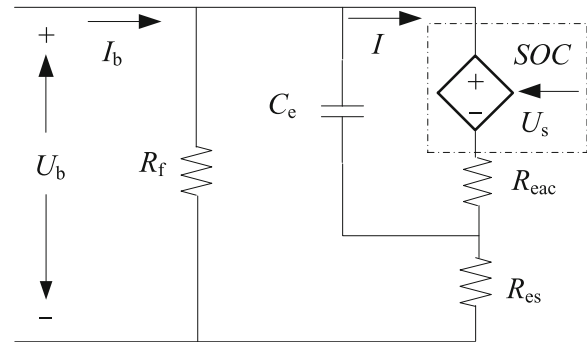

Fig. 1 Equivalent circuit model of VRB

solution impedance and the reaction power equivalent impedance. Many studies have proved that R_{eac} represents 60% of the internal loss with 40% for R_{es} [18–20]. R_f represents the pumping loss and additional loss. C_e represents the interelectrode capacitance, which simulates the transient state process of VRB, and the equivalent capacitance of a single battery is around 6F.

According to the Nernst equation of electrochemical reaction and ignoring the influence of hydrogen ion concentration, the open circuit voltage of a single battery can be described as:

$$U_{cell} = E_0 - \frac{RT}{F} \ln \frac{C_3 C_4}{C_2 C_5}. \tag{1}$$

In (1), U_{cell} is the open circuit voltage of the battery cell, and its unit is V. C_i ($i = 2,3,4,5$) represents the concentration of vanadium ion in each valence state, and its unit is mol·L^{-1}. T is the absolute temperature with unit of K, and R represents the ideal gas constant and is given as 8.314 J·K^{-1}·mol^{-1}. F represents the Faraday constant and equals to 96,500 C·mol^{-1}. When the temperature is 298 K, the positive and negative electrode potential E_0 between the positive and negative electrodes of VRB is:

$$E_0 = E_{0+} - E_{0-} = 1.004 - (-0.225) = 1.259(V), \tag{2}$$

SOC represents the charge state of VRB and is given as:

$$SOC = \frac{E_S}{E_C}. \tag{3}$$

where E_s and E_c are the remaining energy and rated capacity of the battery, respectively. The range of SOC is 0 to 1. When $SOC = 0$, the battery is empty, and when $SOC = 1$, the battery is full. SOC can be expressed as a ratio of ionic concentration when the concentration of positive ions equal to the negative.

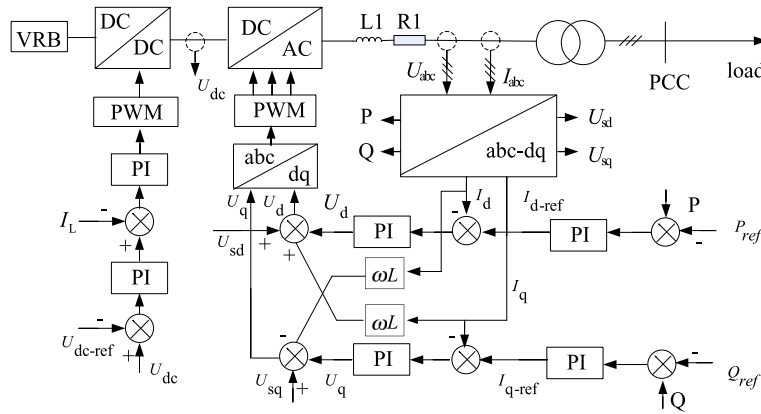SOCs for the negative electrolyte and positive electrolyte are given as:

Zhou *et al. Protection and Control of Modern Power Systems* (2018) 3:32

Page 3 of 13

Fig. 2 Control principle of VRB energy storage system

$$SOC_n = \frac{C_2}{C_3 + C_2} \tag{4}$$

$$SOC_p = \frac{C_5}{C_5 + C_4} \tag{5}$$

When the positive and negative reactions are balanced, the hydrogen concentration is approximately a constant, i.e. $SOC = SOC_n = SOC_p$. Therefore, the VRB circuit voltage can be described as:

$$U_{\text{cell}} = 1.259 - \frac{RT}{F} \ln \left(\frac{1 - SOC}{SOC} \right)^2 . \tag{6}$$

SOC changes with the battery charging and discharging as:

$$SOC_{t+1} = SOC_t + \Delta SOC \tag{7}$$

$$\Delta SOC = \frac{\Delta E}{E_C} = \frac{P_s \Delta t}{E_C} = \frac{I U_S \Delta t}{E_C} \tag{8}$$

In the above equations, Δt represents the time step, SOC_{t+1} and SOC_t are the SOC states of the battery at t + 1 and t instants, respectively. ΔE is the total energy change of the battery and ΔSOC represents the change of the SOC at one time step.

Generally, the voltage of the VRB monomer is not high. In order to match the system voltage, multiple monomers are connected in series to form a stack. For a VRB stack with N_{cell} numbers of VRB monomers, its open circuit voltage can be described as:

$$U_S = N_{\text{cell}} U_{\text{cell}} \tag{9}$$

2.2 VRB energy storage system
2.2.1 Construction of VRB energy storage system
The VRB energy storage system contains a VRB, a converter, and a filter. As VRB outputs DC, a DC/AC converter is required for integrating to the power grid. In this paper, the VRB is connected to the power grid by a bidirectional DC/DC converter, a DC/AC converter and a LC filter.

The bidirectional DC/DC converter adopts Boost-Buck circuit with dual-loop control strategy including a voltage outer loop and current inner loop to achieve bidirectional fast energy flow [21, 22]. The DC/AC converter also adopts dual-loop decoupling control strategy with power outer loop and current inner loop [23]. The active power reference P_{ref} is the difference between the output active power and the required active power of the grid, and the obtained error is fed to the PI regulator to generate the reference value of the d-axis current. The reference value of reactive power Q_{ref} is set to 0 to ensure unit power factor. When the VRB charges, $P_{ref} < 0$, and the control signal causes the DC/AC inverter to operate in rectifier state, and the DC/DC converter in the BUCK mode. When the VRB discharges, $P_{ref} > 0$, the DC/AC converter operates in inverter state and the DC/DC converter in the BOOST mode.

The block diagram of the overall control diagram of the VRB energy storage system is shown in Fig. 2. L_1 and R_1 are the filter inductance and resistance, respectively.
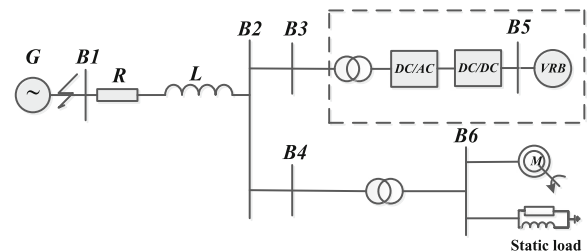

Fig. 3 Grid simulation structure diagram of VRB

Zhou *et al. Protection and Control of Modern Power Systems* (2018) 3:32
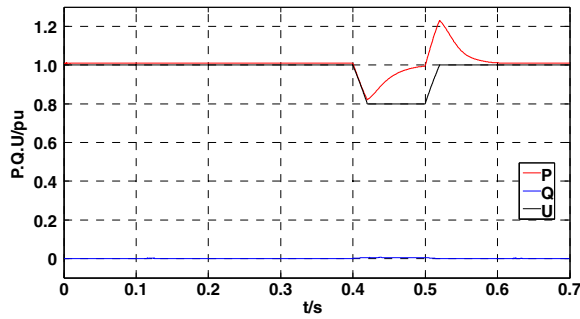
Page 4 of 13

Fig. 4 External characteristics of VRB energy storage system

2.2.2 Grid simulation

Based on the previous descriptions, Matlab/Simulink is used to construct the simulation system shown in Fig. 3. The load characteristics of the VRB energy storage system can be obtained by measuring the data at the bus B3.

In Fig. 3, the induction motor simulates the dynamic load, the resistance load in parallel with the inductance load simulate the static load, and the VRB energy storage system is connected to the distribution network through the DC/DC and DC/AC converters. L and R represent the network parameters.

3 Equivalent description of VRB energy storage system

Establishing an equivalent mathematical model describing the external characteristics of VRB energy storage system to meet the demand of power grid simulation is required to study the synthesis load model of distribution network including VRB. An appropriately simplified model is not only a guarantee for accurate power system simulation, but also an essence for reducing simulation difficulty [24]. In this paper, the equivalent model of the VRB energy storage system is established based on the principle of VRB external characteristic fitting.

3.1 Dynamic characteristics of VRB

In order to study the dynamic characteristics of the VRB energy storage system, the system established in the last section is connected to a power grid. A series of voltage disturbances are applied to test the system. In the process of VRB charging and discharging, three-phase short-circuit faults are applied at bus B1 (see Fig. 3) to cause voltage drops of 10% to 40%. The load data at B3 (active power, reactive power and bus voltage) are measured and the dynamic characteristics of the VRB energy storage system in transient process are obtained. Taking the 20% voltage drop as an example, the dynamic characteristic curve of the VRB energy storage system is shown in Fig. 4.

In Fig. 4, in the transient of bus voltage drop, the variation of the reactive power of the VRB energy storage system is very small, and its value is close to 0. Therefore, to simplify the model, the reactive power is fixed at zero in this paper. The active power P_{VRB} is no longer a constant, and in a dynamic state, the static constant power load cannot describe its transient characteristics accurately, and it must be equivalent to the generalized dynamic load.

3.2 Equivalent description model of VRB

Previous analysis shows that it is necessary to establish a dynamic equivalent model to describe the transient characteristics of the VRB energy storage system accurately. According to Fig. 4, the voltage disturbance of the power system can be regarded as superposition of step excitation signals, and the active power output of the VRB energy storage system is close to the step response of the first-order inertial system. Therefore, the step response of the first-order inertial system is used as the equivalent model of the VRB energy storage system after ignoring the reactive power output of the system as:

Table 1 Recognition results of equivalent model parameters

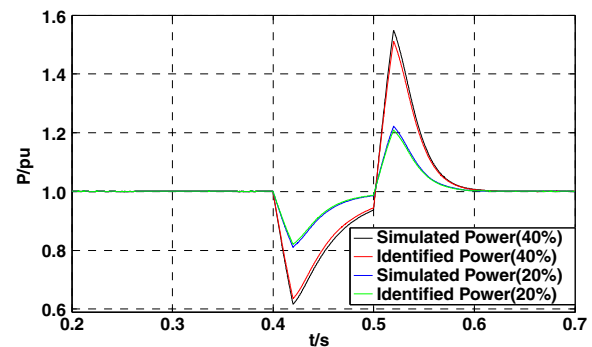| Disturbance	U	T	K_u	E_r
Large disturbance	− 10%	33.27	1.0211	2.484e-3
	− 15%	33.12	1.0445	3.796e-3
	−20%	32.39	1.0712	5.297e-3
	−25%	32.02	1.0976	6.122e-3
	−30%	31.58	1.1246	8.233e-3
	−40%	30.63	1.1969	9.568e − 3
Continuous small disturbance	-3%,+ 7%,-5%, + 2%,-3%,+ 1%	29.20	1.0215	2.600e-3

Fig. 5 Fitting curves of the model under large disturbance

$$P_{VRB} = 2P_0 - P_0\left[\frac{u}{\tau s + 1} + K_u(u - U_0)\right] \quad (10)$$

In (10), P_0 represents the initial active power output of the VRB energy storage system and is set as the rated power P_{NVRB}. The steady-state maximum output active power of the model is P_{NVRB}, so this model can simulate the limit output of the VRB energy storage system accurately. u and U_0 represent the actual and initial values of the system voltage, respectively, and U_0 equals to the rated voltage U_N. τ represents the inertial time constant of the system and K_u is the voltage compensation factor.

This model uses the first-order transfer function of voltage to represent the real-time active power output of the VRB energy storage system. The model has limited parameters and the structure is simple, which make the model easy to realize in power simulation software.

3.3 Verification of equivalent model of VRB energy storage system

Voltage disturbances can be divided into large disturbance and continuous small disturbance according to the different degrees. When different voltage disturbances occur, the genetic algorithm [25, 26] can accurately and quickly identify the parameters of the model, and the output response of the model can then be obtained. The effectiveness of the equivalent VRB model is verified by comparing the output response with the load characteristics of the VRB energy storage system under same disturbances.

3.3.1 Large disturbance verification

The system shown in Fig. 3 is simulated and the three-phase short-circuit faults are applied at the bus B1 to cause bus voltage drops of 10%–40%. The effective value of the voltage at the bus B3 is the excitation of the model, where the active power curve is the target response curve. The six sets of data as the results of model parameter identification are shown in Table 1.

Experiments on voltage drops of 20% and 40% of bus B1 are carried out in this paper, and the fitting curves are shown in Fig. 5.

3.3.2 Continuous small disturbance verification

Similarly, a continuous small disturbance is applied at bus B1. The voltage fluctuations and the fitting curves are shown in Fig. 6 (a) and (b), respectively. The identification results are also shown in Table 1.
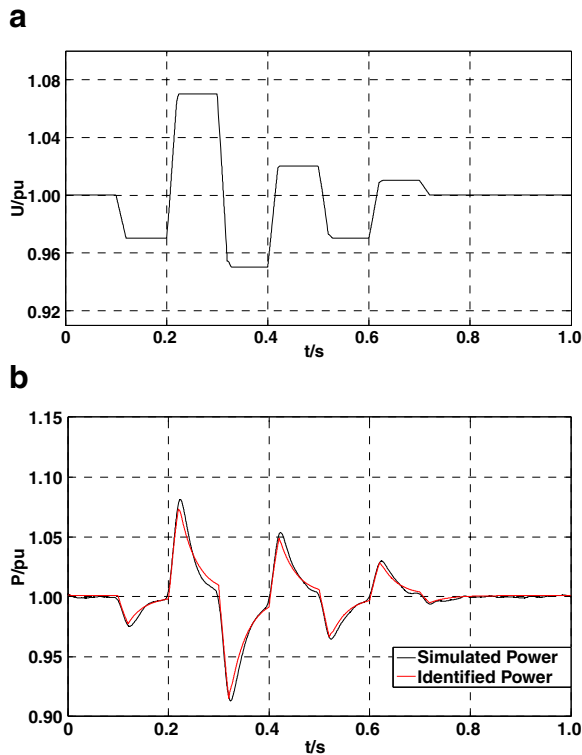

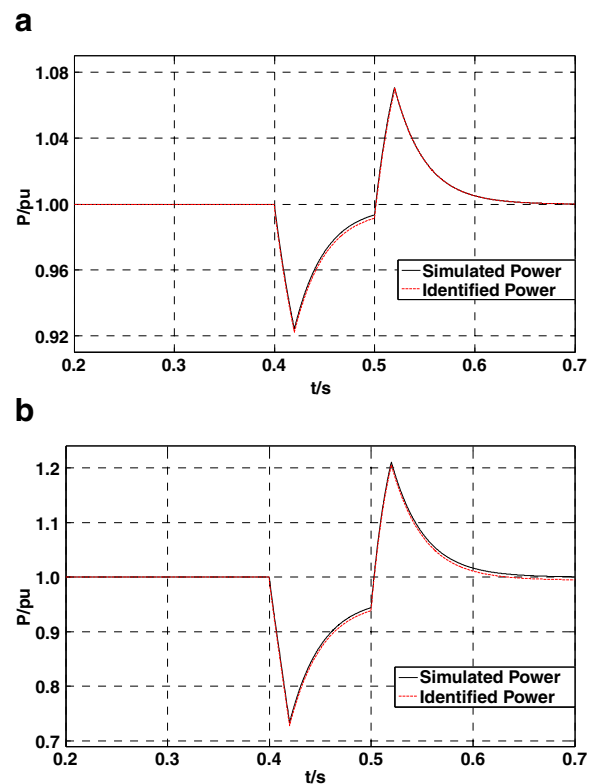**Fig. 6** Voltage disturbance curve and fitting curve of the model under continuous small disturbance

Fig. 7 Interpolation and extrapolation capability verification

Zhou *et al. Protection and Control of Modern Power Systems* (2018) 3:32

Page 6 of 13

Table 2 Response residuals error of interpolation and extrapolation

Algorithm	Interpolation 10%	Extrapolation 30%
residual	2.501e-3	8.593e-3

3.3.3 Result analysis

It is seen from Fig. 5 and Fig. 6 that the model response can be well fitted to the load characteristics of the VRB energy storage system in the transient process under both the large and small voltage disturbances. It shows that the equivalent VRB model proposed in this paper is a good approximation to the data samples and has strong self-description ability. The identification parameters and residuals in Table 1 also support this observation. The above analysis shows that the first-order transfer function model proposed in this paper can accurately describe the load characteristics of the VRB energy storage system.

In Table 1, E_r is calculated according to (11), and its size reflects the degree of the fitting effect. The smaller the E_r is, the better the fitting effect has.

$$E_r = \frac{1}{N} \sum_{k=0}^{N} \sqrt{(P_S(k) - P_1(k))^2} \tag{11}$$

In (11), $P_s(k)$ is the actual response of the simulation system, N is the measured data length, and $P_1(k)$ represents the identification responses.

3.3.4 Generalization ability test of model

The model with the parameters identified under voltage drop of 20% at the bus B1 fits the response curves of the model obtained under bus voltage drop of 10% (interpolation capability validation) and 30% (extrapolating ability validation). The generalization ability of the model is verified by comparing the fitting degree of the corresponding model response to the simulation response. The curve of interpolation and extrapolation is shown in Fig. 7, and the fitting residuals are shown in Table 2. The results show that although the voltage excitation amplitudes of the fitting sample and the modeling sample are different, the model has good interpolation and generalization abilities.

It should be pointed out that load model parameter identification is a typical nonlinear mathematical problem, and no optimization algorithm can guarantee the uniqueness of the results. Therefore, it is inevitable that the identified model parameters have certain dispersion.
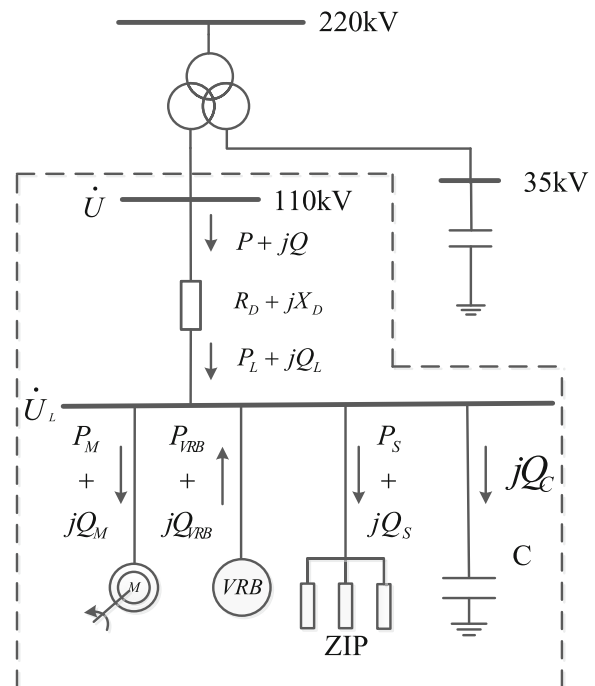

Fig. 8 Structure diagram of GSLM

4 Structure and parameter identification of GSLM

CLM does not take into account the influence of distribution grid parameters. Many modeling practices have shown that induction motors have good ability to represent synthesis load, but the ability to describe the reactive power in the transient process after disturbances is poor. Therefore, a dynamic reactive power compensation device is proposed to connect in parallel with the static load [27]. Reference [28] points out that the structure of generalized load model including energy storage system needs to increase the size of the energy storage system on the virtual bus of the synthesis load model. Large numbers of energy storage system can be regarded as the dynamic load with negative power. A generalized synthesis load model with the VRB energy storage system is established in this paper, which takes into account the influence of distribution network parameters and reactive power compensation equipment.

4.1 The structure of GSLM

The structure of GSLM is shown in Fig. 8, which takes into account the parameters of the distribution network $R_D + jX_D$, the compensation capacitor C and the VRB energy storage system. U and U_L represent

Table 3 Typical value of non-key parameters

R_S	X_r/pu	A_m/pu	B_m/pu	C_m/pu	X_D/R_D	$\cos \varphi$
0.03	0.12	1	0	0	15	0.85

Table 4 Six different load levels

VRB State	Load Level	P/pu	P_{VRB}/pu	P_M/pu	P_S/pu
Discharge	1	0.820	0.606	0.938	0.488
	2	0.108	0.606	0.469	0.245
	3	−0.131	0.606	0.313	0.162
Charge	1	2.045	−0.618	0.940	0.487
	2	1.332	−0.618	0.470	0.244
	3	1.094	−0.618	0.313	0.163

the actual and virtual load bus voltages, respectively, and the part between the actual and virtual buses is the equivalent impedance of the distribution network.

Assuming that the system frequency is at the rated frequency in normal operation, i.e., $f_0 = 1pu$, and in per-unit terms, $X = L$.

1) Distribution network parameters

Considering $U = U\angle 0°$, as shown in Fig. 8, there are:

$$\dot{U}_L^g = \left(U - \frac{PR_D + QfX_D}{U}\right) - j\frac{PfX_D + QR_D}{U} \quad (12)$$

$$\begin{cases} P_D = \dfrac{P^2 + Q^2}{U^2} R_D \\ Q_D = \dfrac{P^2 + Q^2}{U^2} fX_D \end{cases} \quad (13)$$

$$\begin{cases} P_L = P - P_D \\ Q_L = Q - Q_D \end{cases} \quad (14)$$

2) Compensation capacitor

Under the per-unit system:

$$X_C = \frac{1}{\omega C} = \frac{X_{C0}}{f}, X_{C0} = \frac{1}{C}. \quad (15)$$

Therefore, the capacity of the compensation capacitor is:

$$Q_C = -\frac{U_L^2}{X_C} = -\frac{U_L^2}{X_{C0}} f. \quad (16)$$

where X_{C0} represents the capacitive reactance in normal operation and can be obtained as:

$$X_{C0} = -\frac{U_{L0}^2}{Q_{C0}} \quad (17)$$

$$C = \frac{1}{X_{C0}} = -\frac{Q_{C0}}{U_{L0}^2} \quad (18)$$

If $X_{C0} > 0$, this part is a real reactive compensation equipment, otherwise, this part is a reactive load and can be incorporated into the static load.

3) ZIP

The static load is equivalent to a constant admittance ($Y = G-jB$, and if $B > 0$, Y is an inductive load):

$$\begin{cases} P_{ZIP} = GU_L^2 \\ Q_{ZIP} = BU_L^2 \end{cases} \quad (19)$$

4) Motor

The induction motor has the dynamic characteristics represented by the third-order dynamic differential equations under the synchronous coordinate system. This model is widely used so no further discussion is given here.

4.2 Unknown parameters of GSLM

In Fig. 8, P_M, Q_M, P_{VRB}, Q_{VRB}, P_S, Q_S, and Q_C represent the active and reactive powers of the induction motor, active and the reactive powers produced by the VRB, active and reactive powers of the static load, reactive power of the compensation capacitor, respectively. The arrows in Fig. 8 represent the reference power directions, and positive power means the direction of the actual power is the same as the reference direction, and vice versa. As can be seen from the previous section, GSLM has a total of 18 parameters, i.e., R_D, X_D, X_M, R_S, X_S, R_r, X_r, T_j, A_m, B_m, C_m, G, B, X_{C0}, the ratio of the system reference power to the reference power of the induction motor K [13], T and Ku of the equivalent model, and the proportion of the VRB energy storage system $K_{VRB} = P_{VRB}/(P_m + P_S)$.

According to [29–31], some of the parameters in the model are difficult to identify and the identification results are discrete. The identification strategy used in this paper only identifies the values of the key parameters, whereas typical values are used for other parameters. Sensitivity analysis shows that among the motor parameters, only K, X_S, R_r, X_m, and T_j have relatively large sensitivity, and thus, typical values are used for other motor parameters.

For the distribution network parameters, the parameters of GSLM cannot be uniquely identified when R_D and X_D are unknown. However, when one of their

Zhou *et al. Protection and Control of Modern Power Systems* (2018) 3:32

Page 8 of 13

values or the relation between them (X_D/R_D) is known, the parameters of GSLM is uniquely identifiable [32]. According to the actual statistics, $X_D/R_D = 15$ is used in this paper.

The compensation capacitor X_C is calculated as previous described. If X_C is not considered separately, the power factor of static load may become abnormal and the calculation results become unreasonable. In order to separate X_C from the static load, additional condition is required. To ensure normal power factor for the static load, it is assumed that the power factor $cos\varphi$ is known. As $B/G = tan\varphi$, the relationship between G and B is thus known and X_C can be determined once G and B are obtained.

Thus, there are 10 key unknown parameters, i.e., X_S, R_r, X_m, T_j, K, G, X_D, K_{VRB}, T, and K_u. Other parameters can take typical recommended values from China Electric Power Research Institute, as shown in Table 3.

Table 5 Recognition results of generalized synthesis load model parameters

VRB state	Load level	ΔU	X_s	R_r	X_m	T_j	K	G	X_D	K_{VRB}	T	K_u	X_C	E_R
Discharge	1	10%	0.052	0.0080	5.058	2.529	1.582	0.336	0.0065	0.359	27.35	1.180	−7.61	2.3e-3
		15%	0.055	0.0079	4.916	2.525	1.555	0.307	0.0062	0.341	27.37	1.092	−7.78	3.1e-3
		20%	0.051	0.0078	5.063	2.522	1.479	0.344	0.0064	0.361	26.87	1.033	−7.50	3.5e-3
		30%	0.053	0.0080	4.990	2.497	1.485	0.335	0.0066	0.355	28.12	1.033	−7.48	4.3e-3
		40%	0.054	0.0080	5.070	2.489	1.491	0.329	0.0067	0.367	28.23	1.017	−7.24	5.4e-3
	σ	/	0.002	0.0001	0.066	0.018	0.047	0.014	0.0002	0.010	0.57	0.067	0.20	/
	2	10%	0.074	0.0079	6.576	2.482	2.655	0.205	0.0081	0.798	22.09	0.934	−9.58	2.0e-3
		15%	0.079	0.0085	6.694	2.417	2.670	0.208	0.0092	0.796	22.95	0.994	−9.36	2.6e-3
		20%	0.077	0.0087	6.767	2.821	2.571	0.192	0.0086	0.790	23.68	1.084	−9.90	3.4e-3
		30%	0.078	0.0078	6.659	2.539	2.597	0.206	0.0088	0.786	23.95	1.018	−9.44	4.2e-3
		40%	0.076	0.0081	6.781	2.672	2.537	0.197	0.0096	0.781	24.39	0.959	−9.67	5.1e-3
	σ	/	0.002	0.0004	0.084	0.161	0.056	0.007	0.0006	0.007	0.91	0.058	0.21	/
	3	10%	0.160	0.012	3.264	7.438	2.558	0.317	0.0408	1.696	26.03	0.951	11.91	3.2e-3
		15%	0.110	0.009	2.493	6.078	3.091	0.289	0.0489	1.680	24.77	1.050	14.35	3.9e-3
		20%	0.152	0.010	2.635	6.492	2.462	0.309	0.0588	1.616	23.05	1.056	12.44	4.8e-3
		30%	0.136	0.011	2.785	6.335	2.896	0.310	0.0449	1.669	24.95	1.016	13.56	5.0e-3
		40%	0.166	0.011	3.038	6.229	2.692	0.294	0.0342	1.619	25.42	1.105	13.71	5.2e-3
	σ	/	0.022	0.001	0.310	0.538	0.255	0.012	0.0092	0.036	1.12	0.057	0.99	/
Charge	1	10%	0.156	0.0228	4.971	0.752	0.550	0.522	0.0214	−0.516	28.29	0.970	9.20	2.6e-3
		15%	0.154	0.0245	4.631	0.782	0.561	0.521	0.0232	−0.524	26.68	1.044	10.51	3.1e-3
		20%	0.167	0.0241	4.731	0.795	0.518	0.539	0.0230	−0.520	23.37	1.085	9.28	3.7e-3
		30%	0.165	0.0224	4.691	0.778	0.531	0.529	0.0231	−0.524	25.91	1.056	9.59	4.1e-3
		40%	0.161	0.0232	4.669	0.783	0.578	0.525	0.0229	−0.517	24.85	1.013	10.93	5.2e-3
	σ	/	0.006	0.0009	0.135	0.016	0.024	0.007	0.0007	0.004	1.86	0.044	0.78	/
	2	10%	0.056	0.0097	3.160	3.511	2.039	0.352	0.0677	−1.000	22.82	1.117	7.90	3.0e-3
		15%	0.052	0.0093	3.201	3.468	2.121	0.339	0.0668	−0.988	23.06	1.016	8.92	3.5e-3
		20%	0.055	0.0089	3.095	3.495	2.026	0.369	0.0701	−0.996	24.12	1.009	7.09	4.5e-3
		30%	0.055	0.0096	3.155	3.609	2.008	0.401	0.0689	−0.989	22.98	1.120	6.43	5.2e-3
		40%	0.054	0.0089	3.150	3.521	2.112	0.355	0.0694	−1.002	23.25	1.007	7.67	5.3e-3
	σ	/	0.002	0.0004	0.038	0.053	0.052	0.024	0.0013	0.006	0.51	0.059	0.93	/
	3	10%	0.046	0.0077	2.206	2.949	3.767	0.258	0.0468	−1.285	26.26	1.079	8.18	3.0e-3
		15%	0.044	0.0080	2.211	2.950	3.789	0.249	0.0455	−1.301	25.69	1.059	8.46	4.5e-3
		20%	0.050	0.0078	2.195	2.890	3.745	0.239	0.0466	−1.269	25.98	1.068	8.40	4.8e-3
		30%	0.046	0.0081	2.099	2.996	3.698	0.255	0.0459	−1.275	24.56	1.057	7.9	5.3e-3
		40%	0.048	0.0079	2.203	2.897	3.697	0.244	0.0456	−1.229	23.46	1.065	8.41	5.6e-3
	σ	/	0.002	0.0002	0.047	0.044	0.041	0.008	0.0006	0.027	1.16	0.009	0.23	/

Zhou *et al. Protection and Control of Modern Power Systems* (2018) 3:32

Page 9 of 13

a

b

Fig. 9 Fitting curves of the first load level under discharging state
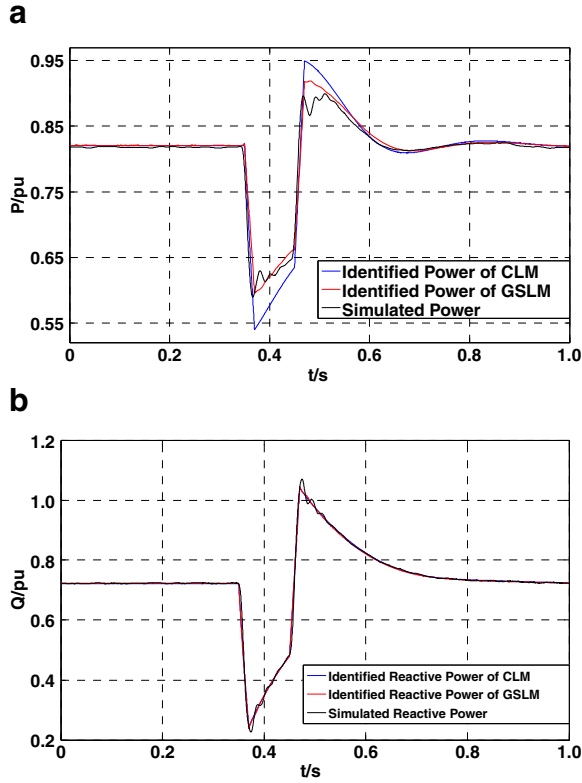
a

b

Fig. 10 Fitting curves of the second load level under discharging state

4.3 Model verification

To verify the complete GSLM model, the voltage at the bus B1 shown in Fig. 3 is dropped by 10%, 15%, 20%, 30% and 40%, respectively, and the model is simulated dynamically under different load levels shown in Table 4. The load data obtained at bus B1 is regarded as the measured sample data, and the parameters are identified by the improved genetic algorithm. The identification results are shown in Table 5, where σ represents the standard deviations of the parameters and E_R represents the fitting error of the dynamic curve.

In Table 4, P, P_{VRB}, P_M, and P_S represent the capacities of the system, VRB energy storage system, dynamic load, and static load, respectively. The fitting effects of the model under the six load levels are described as follows.

4.3.1 Discharge STATE

(1) First load level: $0 < P_{VRB} < P_M$. Under this condition, $K_{VRB} < 1$ and the output power from VRB is insufficient to maintain the load power. The powers of the equivalent dynamic load and static load of the distribution network are supplied by the system, i.e., $P > 0$, and $Q > 0$. From Table 4, the theoretical value of K_{VRB} is
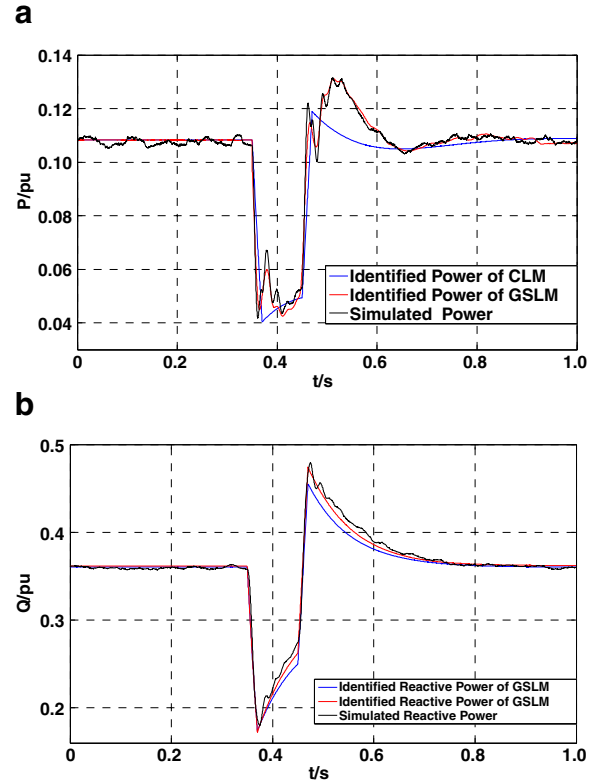
0.425. The fitting effect of the 20% voltage drop under this load level is shown in Fig. 9.

(2) Second load level: $P_M < P_{VEB} < P_M + P_S$. In this condition, $K_{VRB} < 1$, and the output power from VRB fully meets the power absorbed by the induction motor alone, but not the power absorbed by both the induction motor and static load. The theoretical value of K_{VRB} is 0.848 and the fitting effect of the 20% voltage drop under this load level is shown in Fig. 10.

(3) Third load level: $P_{VRB} > P_M + P_S$. Under this condition, $K_{VRB} > 1$, and the output power from VRB fully meets the power required for the total load, and thus the VRB can input a certain amount of active power to the system, i.e., $P < 0$. The theoretical value of K_{VRB} is 1.274 and the fitting effect of the 20% voltage drop under this load level is shown in Fig. 11.

4.3.2 Charge STATE

(1) First load level. The VRB energy storage system acts as a dynamic load to absorb power from the system. The theoretical value of K_{VRB} is − 0.433 and the
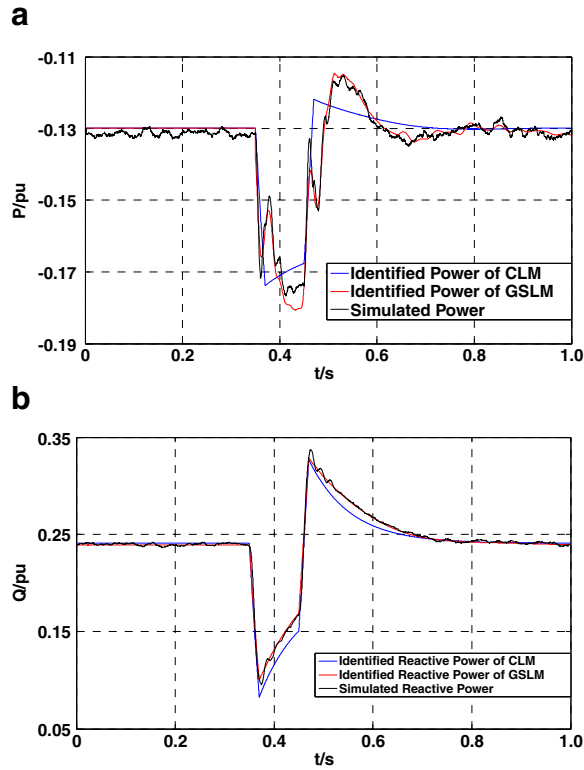
Zhou *et al. Protection and Control of Modern Power Systems* (2018) 3:32

Page 10 of 13

Fig. 11 Fitting curves of the third load level under discharging state

Fig. 12 Fitting curves of the first load level under charging state

fitting effect of the 20% voltage drop under this load level is shown in Fig. 12.

(2) Second load level. The proportion of the output power from the VRB energy storage system increases and the theoretical value of K_{VRB} is − 0.866. The fitting effect of the 20% voltage drop under this load level is shown in Fig. 13.

(3) Third load level. The proportion of the output power from the VRB energy storage system increases further and the theoretical value of K_{VRB} is − 1.298. The fitting effect of the 20% voltage drop under this load level is shown in Fig. 14.

It can be seen from Figs. 9-14 that the GSLM proposed in this paper can effectively describe the external characteristics of the synthesis distribution network load with the VRB under different load levels and different working conditions, and in charging or discharging states. The errors in Table 5 also indicate that the fitting effect is good.

The corresponding fitting effects of GSLM and CLM to the system simulation are also given in Figs. 9-14. Comparing the curves in the figures and the errors in Table 6, the simulation results of GSLM proposed in this paper show much better performance than that of CLM. With the increase of VRB proportion in the
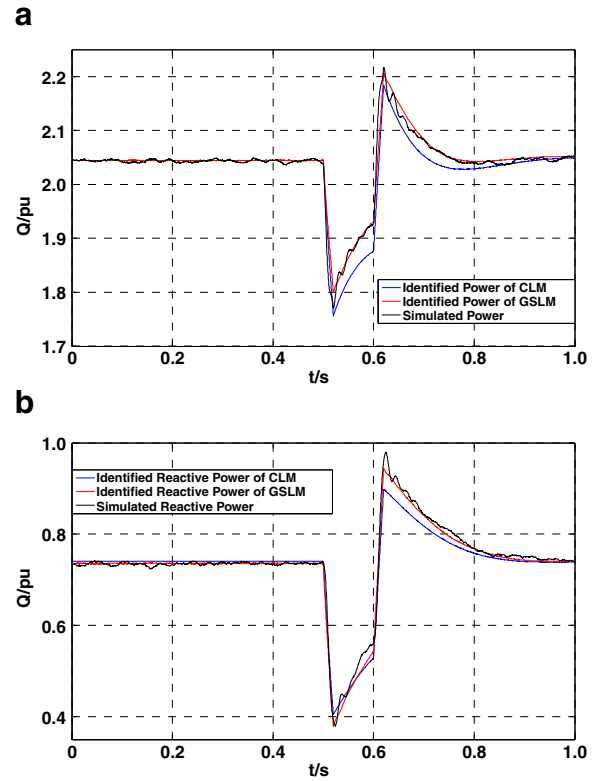
distribution network, the errors of CLM increases, whereas for GSLM, the errors are always smaller.

4.4 Adaptability test of GSLM

(1) Description ability of the model. It can be seen from Figs. 9-14 that compared with the classic synthesis load model, the proposed model can better simulate the simulation data. The errors in Table 5 also show that the fitting residuals are very small for different load levels and voltage disturbances. Therefore, the model has good approximation effect on data samples and good description ability, which can meet the needs of engineering simulation.

(2) The generalization ability of the model. For six different load levels, the model parameters identified under the 20% voltage drop fit the response curves of the model obtained under voltage drops of 10% (interpolation capability verification) and 40% (extrapolation capability verification). The interpolation and extrapolation capability of the model under different voltage conditions is verified. In this paper, the interpolation and extrapolation curves of the
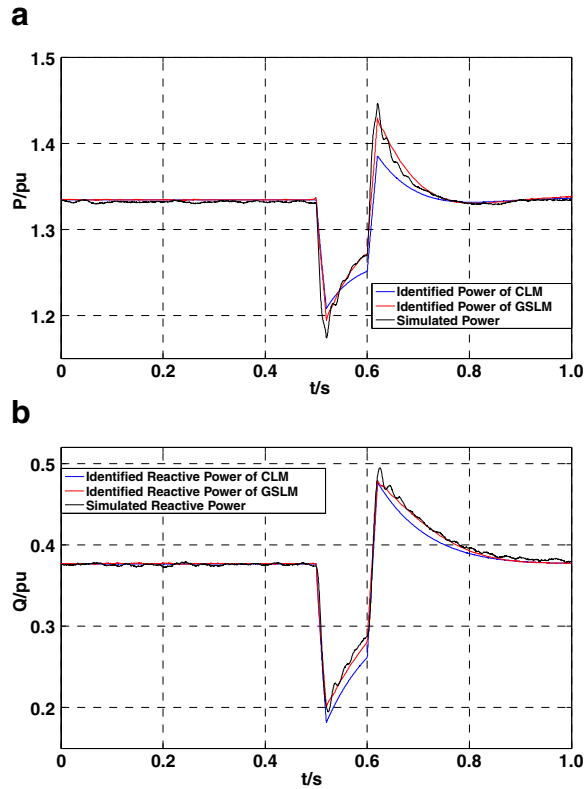
Zhou *et al. Protection and Control of Modern Power Systems* (2018) 3:32

Page 11 of 13

a

b

Fig. 13 Fitting curves of the second load level under charging state

a

b

Fig. 14 Fitting curves of the first load level under charging state

discharge state under first load level are given, as shown in Fig. 15, and the fitting residual results are shown in Table 7. Figure 15 shows that although the amplitudes of the voltage disturbances vary significantly, the responses of the identification results to interpolation and extrapolation sample data are well fitted, as indicated by the residuals in Table 7. The results show that the model has good generalization ability.

(3) Stability analysis of the model parameters. As shown in Table V, except T and X_C, the standard deviations of the parameters are relatively small indicating good parameters stability. The standard deviations of T and X_C are big because their sensitivities are low. Therefore, the overall stability of the model parameters is high.

5 Conclusions

In this paper, the equivalent model, which is the step response of the first-order inertial system, is used to describe the external characteristics of the VRB energy storage system. The model can simulate the m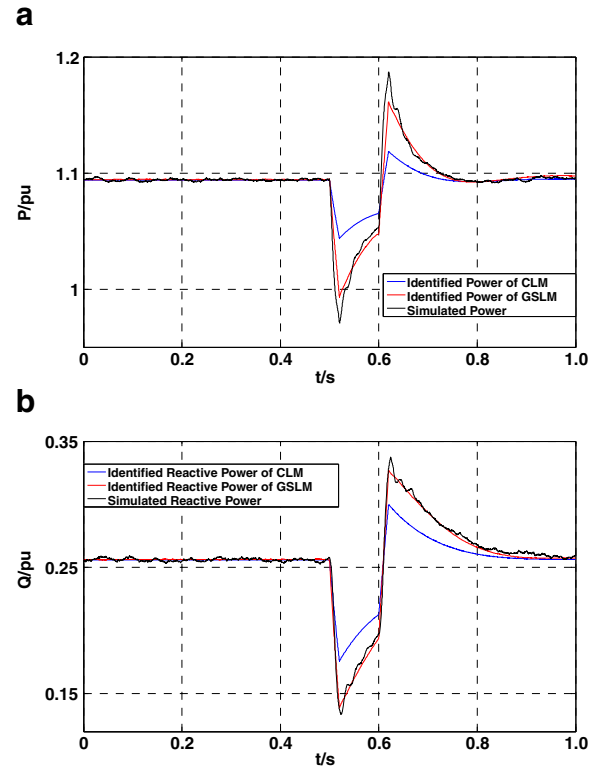aximum output of the VRB energy storage system and fit the external characteristic of the system precisely in the presence of large disturbance and continuous small disturbance. In addition, the model has a simple structure and can be identified easily. On this basis, a generalized synthesis load model (GSLM) with the VRB energy storage system is established, and the distribution network parameters and reactive power compensation are considered. The load characteristics of the distribution network are identified. Simulation results of six typical examples show that GSLM can effectively describe the

Table 6 Error comparison of GSLM and CLM

VRB state	Load level	Model	E_R
Discharge	1	GSLM	3.5e-3
		CLM	9.2e-3
	2	GSLM	3.4e-3
		CLM	2.5e-2
	3	GSLM	4.8e-3
		CLM	2.9e-2
Charge	1	GSLM	3.7e-3
		CLM	1.2e-2
	2	GSLM	4.5e-3
		CLM	2.0e-2
	3	GSLM	4.8e-3
		CLM	2.6e-2

Zhou *et al. Protection and Control of Modern Power Systems* (2018) 3:32
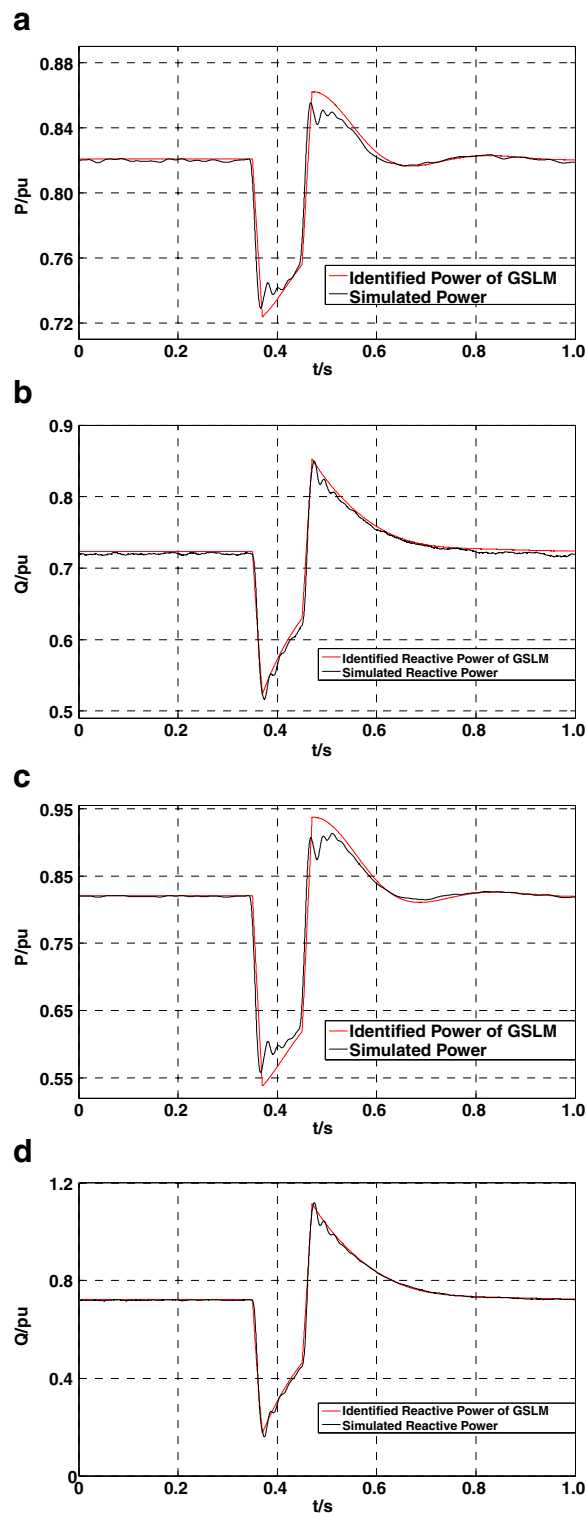
Page 12 of 13

Fig. 15 Interpolation and extrapolation capability verification

Table 7 Response residuals of interpolation and extrapolation

VRB state	Load level	Interpolation 10%	Extrapolation 40%
Discharge	1	2.5e-3	5.7e-3
	2	2.1e-3	5.0e-3
	3	3.3e-3	8.6e-3
Charge	1	2.9e-3	4.8e-3
	2	3.8e-3	5.5e-3
	3	4.6e-3	6.3e-3

load characteristics of the distribution network with energy storage system. Compared with CLM, GSLM has better self-description and generalization ability. The model is effective and has good parameter stability, and the higher the proportion of energy storage in the grid is the better description ability the GSLM has.

Abbreviations
CLM: Classic load model; GSLM: Generalized synthesis load model; VRB: All-vanadium redox flow battery

Availability of data and materials
Data sharing not applicable to this article as no datasets were generated or analysed during the current study.

Authors' contributions
All authors read and approved the final manuscript.

Competing interests
The authors declare that they have no competing interests.

Author details
[1]Guangdong Power Grid Corporation Information Center, Guangzhou, China. [2]College of Electrical and Information Engineering, Hunan University, Changsha 410082, China.

References
1. Navarro, I. R., Samuelsson, O., & Lindahl, S. (2003). Influence of normalization in dynamic reactive load models. *IEEE Transactions on Power Apparatus and Systems, 18*(2), 972–973.
2. Ju, P., Handschin, E., & Karlsson, D. (1996). Nonlinear dynamic load modelling: Model and parameter estimation. *IEEE Transactions on Power Apparatus and Systems, 11*(4), 1689–1697.
3. Hill, D. J. (1993). Nonlinear dynamic load models with recovery for voltage stability studies. *IEEE Transactions on Power Apparatus and Systems, 8*(1), 166–176.
4. Karlsson, D., & Hill, D. J. (1994). Modelling and identification of nonlinear dynamic loads in power systems. *IEEE Transactions on Power Apparatus and Systems, 9*(1), 157–166.
5. Kao, W. S. (2001). The effect of load models on unstable low-frequency oscillation damping in Taipower system experience w/wo power system stabilizers. *IEEE Transactions on Power Apparatus and Systems, 16*(3), 463–472.
6. Pereira, L., Kosterev, D., Mackin, P., Davies, D., Undrill, J., & Zhu, W. C. (2002). An interim dynamic induction motor model for stability studies in the WSCC. *IEEE Transactions on Power Apparatus and Systems, 17*(4), 1108–1115.

Zhou *et al. Protection and Control of Modern Power Systems* (2018) 3:32

Page 13 of 13

7. Ma, J., Renmu, H., & Hill, D. J. (2006). Load modeling by finding support vectors of load data from field measurements. *IEEE Transactions on Power Apparatus and Systems, 21*(2), 726–735.

8. Renmu, H., Ma, J., & Hill, D. J. (2006). Composite load modeling via measurement approach. *IEEE Transactions on Power Apparatus and Systems, 21*(2), 663–672.

9. Badrinarayanan, R., Yu, Z., & Tseng, K. J. (2015). *Performance study of a vanadium redox flow battery (VRB) for use in green data centers* (pp. 1–5). Osaka: IEEE International Telecommunication Energy Conference (INTELEC).

10. Qiu, X., Crow, M. L., & Elmore, A. C. (2015). A balance-of-plant vanadium redox battery system model. *IEEE Transaction on Sustainable Energy, 6*(2), 557–564.

11. Qiu, X., Nguyen, T. A., Guggenberger, J. D., Crow, M. L., & Elmore, A. C. (2014). A field validated model of a vanadium redox flow battery for microgrids. *IEEE Transactions on Smart Grid, 5*(4), 1592–1601.

12. Guggenberger, J. D., Elmore, A. C., Tichenor, J. L., & Crow, M. L. (2012). Performance prediction of a vanadium redox battery for use in portable, scalable microgrids. *IEEE Transactions on Smart Grid, 3*(4), 2109–2116.

13. Shah, A. A., Watt-Smith, M. J., & Walsh, F. C. (2008). A dynamic performance model for redox-flow batteries involving soluble species. *Electrochimica Acta, 53*(27), 8087–8100.

14. Blanc, C., & Rufer, A. (2008). Multiphysics and energetic modeling of a vanadium redox flow battery. In *Proc. IEEE 2008 International Conference Sustainable* pp. 696–701. Singapore: Energy Technol.

15. Kroeze, R. C., & Krein, P. T. (2008). Electrical battery model for use in dynamic electric vehicle simulations. *IEEE Transactions on Power Apparatus and Systems, 23*(4), 1336–1342.

16. Zban, C. J., Wu, X. G., Kromlidis, S., et al. (2003). Two electrical models of the lead-acid battery used in dynamic voltage restorer. *IEEE Proceedings Gener Transm Distrib, 150*, 2175–2182.

17. Chahwan, J., Abbey, C., & Joos, G. (2007). VRB modelling for the study of output terminal voltages, internal losses and performance. In *Electrical Power Conference 2007* (pp. 387–392). Montreal: IEEE Canada.

18. Barote, L., Marinescu, C., & Georgescu, M. (2009). *VRB modeling for storage in stand-alone wind energy systems* (pp. 1–6). Bucharest: PowerTech 2009 IEEE Bucharest.

19. Barote, L., Georgescu, M., & Marinescu, C. (2009). *Smart storage solution for wind systems* (pp. 1–6). Bucharest: PowerTech 2009 IEEE Bucharest.

20. Barote, L., Weissbach, R., Teodorescu, R., Marinescu, C., & Cirstea, M. (2008). Stand-alone wind system with vanadium redox battery energy storage. In *Proc International Conference Optimization Electrical Electron Equipment* (pp. 407–412).

21. Rathore, A. K., Patil, D. R., & Srinivasan, D. (2016). Non-isolated bidirectional soft-switching current-fed LCL resonant DC/DC converter to Interface energy storage in DC microgrid. *IEEE Transactions on Industry Applications, 52*(2), 1711–1722.

22. Amjadi, Z., & Williamson, S. S. (2014). Digital control of a bidirectional DC/DC switched capacitor converter for hybrid electric vehicle energy storage system applications. *IEEE Transactions on Smart Grid, 5*(1), 158–166.

23. García, P., Arboleya, P., Mohamed, B., & Vega, A. A. C. (2016). Implementation of a hybrid distributed/centralized real-time monitoring system for a DC/AC microgrid with energy storage capabilities. *IEEE Transactions on Industrial Informatics., 12*(5), 1900–1909.

24. Korunović, L. M., Sterpu, S., Djokić, S., Yamashita, K., Villanueva, S. M., & Milanović, J. V. (2012). Processing of load parameters based on existing load models. In *Proc 3rd IEEE International Conference Innovative Smart Grid Technologies* (pp. 1–6).

25. Choi, B.-K., Chiang, H.-D., Li, Y. H., Chen, Y.-T., Huang, D.-H., & Lauby, M. G. (2006). Measurement-based dynamic load models: Derivation, comparison, and validation. *IEEE Transactions on Power Apparatus and Systems, 21*(3), 1276–1283.

26. Rudolph, G. (1994). Convergence analysis of canonical genetic algorithms. *IEEE Transactions on Neural Networks, 5*(1), 96–101.

27. Knyazkin, V., Canizares, C. A., & Soder, L. H. (May 2004). On the parameter estimation and modeling of aggregate power system loads. *IEEE Transactions on Power Apparatus and Systems, 19*(2), 1023–1031.

28. Zhu, Y., & Tomsovic, K. (2002). Adaptive power flow method for distribution system with dispersed generation. *IEEE Transactions on Power Delivery, 17*(3), 822–827.

29. Fortes, M. Z., Ferreira, V. H., & Coelho, A. P. F. (2013). The induction motor parameter estimation using genetic algorithm. *Latin America Transactions IEEE, 11*(5), 1273–1278.

30. Duan, F., Živanović, R., Al-Sarawi, S., & Mba, D. (2016). Induction motor parameter estimation using sparse grid optimization algorithm. *IEEE Transactions on Industrial Informatics, 12*(4), 1453–1461.

31. Ju, P., Wu, F., Shao, Z.-Y., Zhang, X.-P., Fu, H.-J., Zhang, P.-F., He, N.-Q., & Han, J.-D. (2007). Composite load models based on field measurements and their applications in dynamic analysis. *IET Generation, Transmission & Distribution, 1*(5), 724–730.

32. Zhou, H. Q., Mao, C., Ju, P., et al. (2008). An identifiability analysis of a synthetic load model with the distribution network considered. *Automation of Electric Power Systems, China, 32*(16), 16–19.